

Numerical Properties of Spherical and Cubical Representative Volume Elements with Different Boundary Conditions

R. Glüge, M. Weber

It has been found that, due to the smaller surface to volume ratio, the spherical representative volume elements (RVE) converge faster to the effective properties than cubical RVEs, in terms of the RVE volume (Glüge et al., 2012). It remains to discuss whether one can actually draw a numerical advantage from this in the finite element calculations, since there are also some drawbacks, for example the necessarily irregular meshing. It has been demonstrated that the boundary conditions, in conjunction with different solution strategies for the linear system that emerges in the FEM, can significantly influence the numerical expense (Fritzen and Böhlke, 2010a). In the light of these results, we examine the numerical properties of spherical and cubical RVEs with linear displacement and periodic (resp. antipodic) boundary conditions.

1 Introduction

The industry requires an ever increasing quality and precision of forming process simulations, while keeping expenses preferably low. This has led to the incorporation of the microstructural properties like texture and grain structure into material models. Unfortunately, the analytical determination of effective properties from the lower-scale structure (homogenization) is restricted to quite elementary problems. Thus, there is a demand for efficient numerical schemes for the determination of effective properties from representative material samples. In many cases, the representative volume element (RVE) method is used, where a (nearly) representative volume element is subjected to some process, and effective material properties are extracted by averaging. The resulting boundary value problem is mostly tackled by the finite element method (FEM). Then, one can use a set of RVE-results as input for the adaption of an effective material law, e.g., with the nonuniform transformation field analysis (Fritzen and Böhlke, 2010b), or even consider the RVEs as material points in large-scale FE simulations (e.g., Feyel (1999); Ilic and Hackl (2009)). Especially for the multiscale FEM approach, the RVE simulations need to be very efficient from a numerical point of view. The question for an numerically optimized RVE is raised, where one may consider different boundary conditions, RVE sizes, RVE shapes and numerical solution strategies. The answer is not as straight forward as one might think. It is for example well known that periodic boundary conditions (PBC) result in a faster convergence in terms of the RVE size, compared to linear displacement boundary conditions (Kanit et al., 2003; Glüge et al., 2012). However, the node coupling in case of PBC increases the bandwidth of the matrix that appears in the linear system in the FEM, which results in higher numerical costs (Fritzen and Böhlke, 2010a). In this work, we address the questions how the RVE-shape affects the numerical properties, specifically the difference between cube and sphere, and discuss different combinations of RVE shapes, boundary conditions and solution techniques exemplarily for a simple homogenization task. Due to the smaller surface to volume ratio, the boundary influence in spherical RVE is smaller than in cubical RVE, which results in a better convergence to the effective material properties in terms of the RVE volume. However, the reduced RVE volume does not result directly in a numerical advantage. Clearly, since the convergence depends on the material and microstructure under consideration, these issues depend on the materials, the microstructure, and the specific FE implementation. However, the case examined in this work may serve as a representative example.

2 Problem Setup

The benchmark problem is the same that has been used for the analysis of convergence in terms of RVE volume in Glüge et al. (2012), briefly summarized in the following sections.

Parameter	Matrix	Inclusion
Young's modulus E in MPa	5000	50000
Poisson's ratio ν	0.4	0.3
Volume fraction	0.7	0.3

Table 1: Material parameters for the matrix and the inclusion material

2.1 RVE and Boundary Conditions

We consider four RVE setups, namely cubical RVEs with periodic boundary conditions, spherical RVEs with antipodic boundary conditions (ABC), and linear displacement boundary conditions on both types. The latter are

$$\mathbf{u} = \overline{\mathbf{H}} \cdot \mathbf{x}_0 \quad \text{on } \partial\Omega \quad (1)$$

where the displacement gradient $\overline{\mathbf{H}}$ is prescribed on the entire boundary of the domain Ω that is occupied by the RVE. The periodic/antipodic boundary conditions require

$$\mathbf{u}^+ - \mathbf{u}^- = \overline{\mathbf{H}} \cdot (\mathbf{x}_0^+ - \mathbf{x}_0^-) \quad (2)$$

$$\mathbf{t}^+ + \mathbf{t}^- = 0 \quad (3)$$

on $\partial\Omega$. The points on the surface are coupled in pairs, where the reference surface normals must satisfy

$$\mathbf{n}_0^+ + \mathbf{n}_0^- = \mathbf{o}. \quad (4)$$

One might consider Eq. (3) basically independent of Eq. (2), since 6 independent equations are needed to complete the boundary value information for two boundary points. However, practically no other choice than Eq. (3) is reasonable. Firstly, static equilibrium requires $\int_{\partial\Omega} \mathbf{t} dA = \mathbf{o}$ and $\int_{\partial\Omega} (\mathbf{x} \times \mathbf{t} - \mathbf{t} \times \mathbf{x}) dA = \mathbf{o}$, and an equal treatment of all boundary points allows only for the application of Eq. (3). Secondly, Eq. (3) is generally adopted automatically in any FE system when imposing Eq. (2), since the node coupling should not contribute to the internal power. The contribution to the stress power p from the coupled points is

$$p = \dot{\mathbf{u}}^+ \cdot \mathbf{t}^+ + \dot{\mathbf{u}}^- \cdot \mathbf{t}^-, \quad (5)$$

which becomes with Eq. (2)

$$p = \underbrace{\dot{\mathbf{u}}^+ \cdot (\mathbf{t}^+ + \mathbf{t}^-)}_{p_{\text{coupling}}} - \underbrace{\mathbf{t}^- \cdot \overline{\mathbf{H}} \cdot (\mathbf{x}_0^+ - \mathbf{x}_0^-)}_{p_{\text{external}}}, \quad (6)$$

where the first term does not involve the external loading. Since the coupling, as a constraint, should not contribute to the stress power, Eq. (3) follows from $p_{\text{coupling}} = 0$ for all possible deformations. Last but not least, only this choice guarantees compliance with the Hill-Mandel-condition (Glüge et al., 2012).

Applied to a cube, one mostly couples opposing surface points such that a periodicity frame emerges, thus the denomination as *periodic boundary conditions*. However, the periodic coupling may also be shifted in order to rotate the periodicity frame (Coenen et al., 2012) or such that no periodicity frame is induced. On the sphere, the coupling is unique: only antipodic points have opposing surface normals. Interestingly, the coupling equations are the same in all cases. The (non-)periodicity depends on the assignment of pairs of surface points. Therefore, it might be clearer to speak of coupled boundary conditions when one refers to the Eqs. (2) and (3) alone.

2.2 Materials and Microstructure

We used the same material and RVE description as published in Glüge et al. (2012), in order to take advantage of a large set of existing RVE results. The material under consideration is a matrix-inclusion material. The matrix is isotropic and linearly elastic. The inclusions, with a total volume fraction of 0.3 are spherical, isotropic, linearly elastic particles of equal diameter, distributed uniformly without preferred alignment or pattern. They are considerably stiffer than the matrix material. The material parameters are collected in Table 1.

	approx. No. of incl.	total No. of nodes	approx. No. of nodes per incl.	No. of surface nodes	No. of DOF for linear disp. BC	No. of DOF for periodic/antipodic BC
spherical RVE	2.4	4462	1858	962	10500	11943
	4.7	7992	1704	1538	19362	21669
	11.1	17832	1604	2562	45810	49653
	19.2	31478	1639	3650	83484	88959
	28.2	45794	1625	4930	122592	129987
	37.5	59926	1598	5642	162852	171315
cubical RVE	4.6	4916	1072	1538	10134	12441
	9.0	9264	1034	2402	20586	24189
	21.2	21171	998	4268	50709	52656
	36.7	35940	980	6146	89382	98601
	53.8	50656	941	7778	128634	140301
	71.62	68924	962	9602	177966	192369

Table 2: RVE and mesh sizes that have been tested.

2.3 Test Setup

We carried out uniaxial tension tests, in which the effective Young’s modulus is to be determined. The latter is accomplished by imposing most components of the average displacement gradient,

$$\bar{H}_{(uax)ij} = \begin{bmatrix} \varepsilon & 0 & 0 \\ 0 & - & 0 \\ 0 & 0 & - \end{bmatrix}. \quad (7)$$

Not prescribing $\bar{H}_{(uax)22}$ and $\bar{H}_{(uax)33}$ results in zero stress components \bar{T}_{22} and \bar{T}_{33} of the effective first Piola-Kirchhoff-stresses, which are stress-power-conjugate to \bar{H} . Young’s modulus is given by

$$E = \bar{T}_{11}/\varepsilon, \quad (8)$$

where ε needs to be small.

2.4 Numerical Setup

For the FE simulations, we employed hexahedral eight-node bricks with linear shape functions for the meshing, which is regular in case of the cubical RVE (see Fig. 1). The microstructure has been accounted for by the Gauss-point-method (Kreikemeier, 2012), where the largest element size has been constrained to one eighth of the inclusion diameter. The inclusions have been dispersed randomly in the RVE, where intersections with the RVE boundary have been allowed, disregarding the periodicity frame. The volume fractions have been ensured by trial and error distributions. To impose an average displacement gradient \bar{H} , three additional nodes have been used, the three degrees of freedom (DOF) of which appear in the constraint equations. These equations allow for a linear coupling of arbitrary DOF, which serve for the implementation of the displacement boundary conditions (Eqs. (1) and (2)). The simulations have been conducted on an eight-core Intel I7-950 CPU¹, using the FE system ABAQUS 6.10-2 and its iterative and direct solver. Different RVE-sizes have been examined, the parameters of which are collected in Table 2. One can already notice that the number of nodes per inclusion is approximately 1.7 times larger for the spherical RVE. This is due to the common element size limit. The cube is meshed regularly with cubical elements, while the meshing of the sphere requires smaller and distorted elements. For numerical parameters like tolerances and precisions, ABAQUS default values have been used.

2.4.1 Influence of the Type of Boundary Condition on the Numerical Problem

Firstly, the linear displacement boundary conditions require twice the number of constraint equations, compared to the periodic/antipodic boundary conditions. Presuming that each constraint equation is used to eliminate a DOF,

¹Linux 3.2.0-33-generic x86-64 GNU/Linux with Intel Fortran 12.0.4

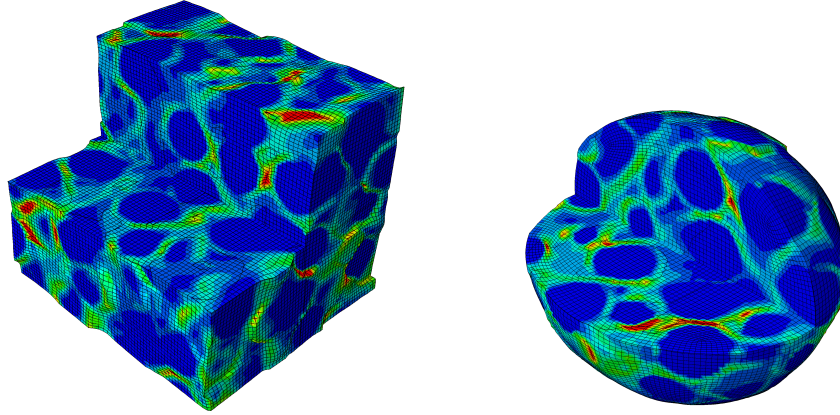


Figure 1: Deformed cubical and spherical RVE with periodic and antipodic boundary conditions, one fourth is cut out. The color map indicates the accumulated plastic strain from 0 (blue) to 0.2 (red).

one has a slightly reduced number of DOF in case of the linear displacement boundary conditions. Secondly, the node coupling for the periodic/antipodic boundary conditions induces an increase of the system matrix bandwidth, see Fritzen and Böhlke (2010a). For some matrix storage schemes and solvers, this can result in a severe decrease of performance.

2.4.2 Influence of the RVE Shape on the Numerical Problem

Taking the cubical RVE as reference, there are two competing effects when going to spherical RVE. Capturing the same volume requires approximately 19% less surface, hence one may expect a corresponding reduction of the number of surface nodes. However, this holds only when both types of RVE are meshed the same way, i.e. both regularly or irregularly. In the present example, the cube is meshed regularly. With hexahedral elements, this is not possible on spherical RVE. With a common maximum permitted element length, one has a higher density of surface points on the sphere. Thus, the overall reduction of surface points is only approximately 8% (see Table 2, largest spherical and third-largest cubical RVE).

3 Results

For most calculations, the iterative solver performs better than the direct solver, regarding the time per iteration as well as memory requirements. Only in case of relatively small FE models the direct solver is slightly faster. The largest ratio $t_{\Delta_{\text{direct}}}/t_{\Delta_{\text{iterative}}}$ (timer per iteration using the direct solver over timer per iteration using the iterative solver) is obtained as approximately 7.5 for the largest cubical RVE with periodic boundary conditions.

3.1 Effect of the Type of Boundary Condition and RVE Shape on the the Solver Performance

Time per iteration Regarding the time per equilibrium iteration, there is no notable difference between spherical and cubical RVE in case of linear displacement boundary conditions. Only the total number of DOF is relevant. Going from linear displacement boundary conditions to periodic/antipodic boundary conditions, a slight decrease of performance is observed for the iterative solver, while the direct solver displays a more pronounced decrease of performance. The results are depicted in Fig. 2. The leading coefficients of the quadratic and linear regressions on the data points (time per iteration in seconds over the number of DOF) are summarized in Table 3. For the direct solver, the leading coefficients in the quadratic regressions differ by a factor of approximately 2.97 for the spherical and by approximately 4.9 for the cubical RVE when going from linear displacement to periodic/antipodic boundary conditions, while for the iterative solver these ratios are with 1.19 for the sphere and 1.09 for the cube close to one.

Memory usage ABAQUS estimates a minimum and an optimum amount of required memory, where for the latter the read and write activity from and to the hard disk is minimized. The memory usage is plotted in Fig. 3

RVE setup	direct	iterative
spherical, LDBC	$0.007199 \cdot 10^{-6}$	$0.78682 \cdot 10^{-3}$
spherical, PBC	$0.021426 \cdot 10^{-6}$	$0.93816 \cdot 10^{-3}$
cubical, LDBC	$0.006468 \cdot 10^{-6}$	$0.83013 \cdot 10^{-3}$
cubical, PBC	$0.031925 \cdot 10^{-6}$	$0.90690 \cdot 10^{-3}$

Table 3: Leading coefficients in the quadratic (direct solver) and linear (iterative solver) regression functions for the CPU time per iteration in seconds over number of DOF for the different RVE setups.

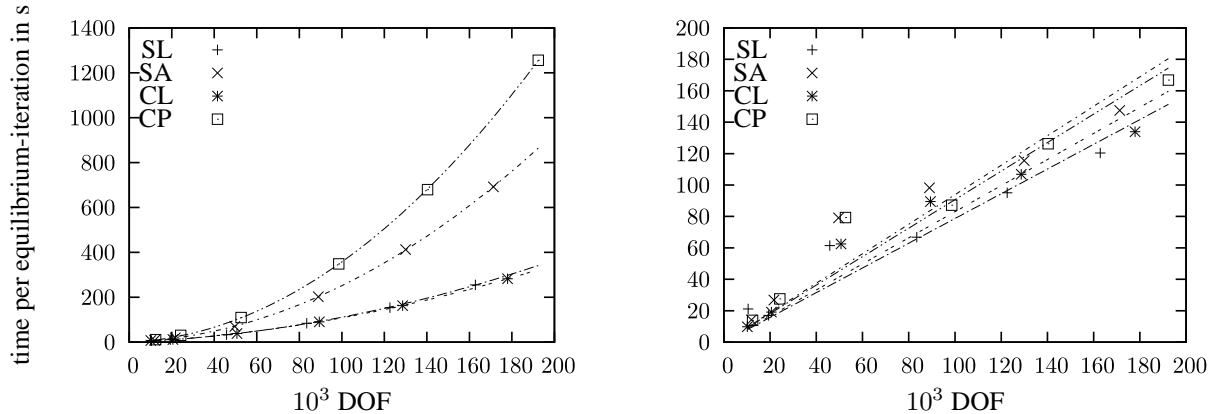


Figure 2: Time per equilibrium iteration over the number of degrees of freedom needed by the direct (left) and iterative (right) solver for the different RVE setups. In the legend, S and C stand for sphere and cube, while L, P and A stand for linear displacement, periodic and antipodic boundary conditions.

for different RVE setups and solvers. The minimum memory requirements are similar for both solver types, and relatively insensitive to the RVE shape.

Iterative solver: It turns out that the memory requirements of the iterative solver are insensitive both to the kind of boundary condition and the shape of the RVE. The ratio of the optimum to the minimum memory usage is rather small, and lies mostly below 1.4.

Direct solver: While insensitive to the RVE shape, the minimum memory requirement is approximately doubled when going from linear displacement to periodic/antipodic boundary conditions. The optimal memory usage depends highly on the boundary conditions and the RVE shape: it is insensitive to the shape of the RVE in case of linear displacement boundary conditions, but sensitive to the RVE shape when periodic/antipodic boundary conditions are used. Similarly to the increase of time per iteration, the node coupling due to periodic/antipodic boundary conditions increases the memory usage. This behaviour is more pronounced for the cubical RVE, since the ratio of coupled DOF to the overall number of DOF is, due to the greater surface to volume ratio, larger than for the spherical RVE. In any case, the optimum memory required is considerably higher than the minimum memory requirement, at least by a factor of 3.5.

3.2 RVE Quality

One can estimate the overall RVE quality by relating the precision of the effective material to the numerical expense. Here, we use the absolute value of the relative deviation of E_{RVE} from the asymptotic Young's modulus E_∞ , $|(E_\infty - E_{RVE})|/E_\infty$, as the error estimate. Plotting this measure over the time per iteration gives a clear picture of which RVE/boundary condition/solution technique is most advantageous, see Fig. 4. Each data point is the result of an averaging over 100 RVE simulations with different inclusion distributions. E_∞ has been taken as the average of the results of the largest spherical and cubical RVE.

One sees immediately that the numerical extra-costs of periodic/antipodic boundary conditions instead of linear displacement boundary conditions pay off, regardless of solver type and RVE shape. The convergence is quite fast when PBC/ABC are applied. The advantage of the spherical RVE over the cubical RVE observed in Glüge et al. (2012) is almost cancelled out by the higher number of nodes per volume, due to the irregular meshing of the sphere. Still, especially for small RVE, the effective properties are estimated more efficiently for spherical RVE.

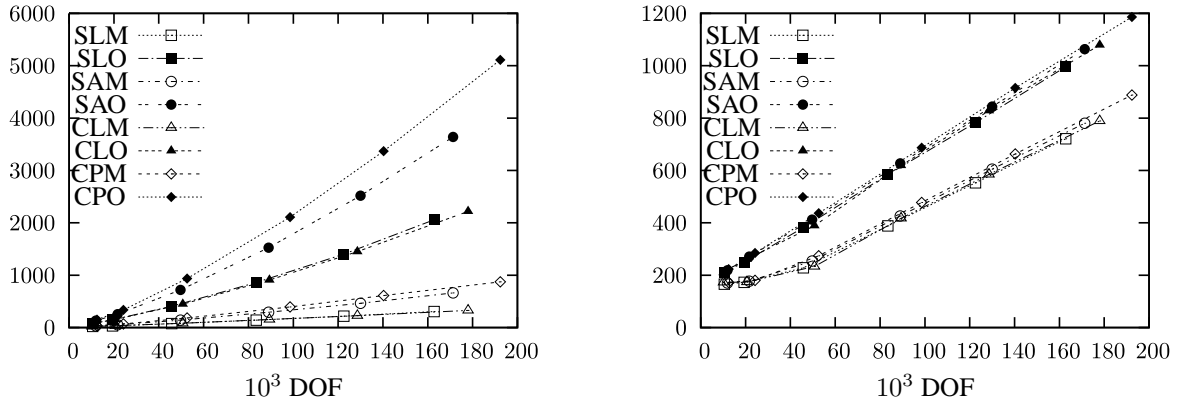


Figure 3: Memory usage over the number of degrees of freedom for different RVE setups for the direct (left) and iterative (right) solver. In the legend, S and C stand for sphere and cube, while L, P and A stand for linear displacement, periodic and antipodic boundary conditions, and M and O stand for the minimum and optimum performance memory requirement.

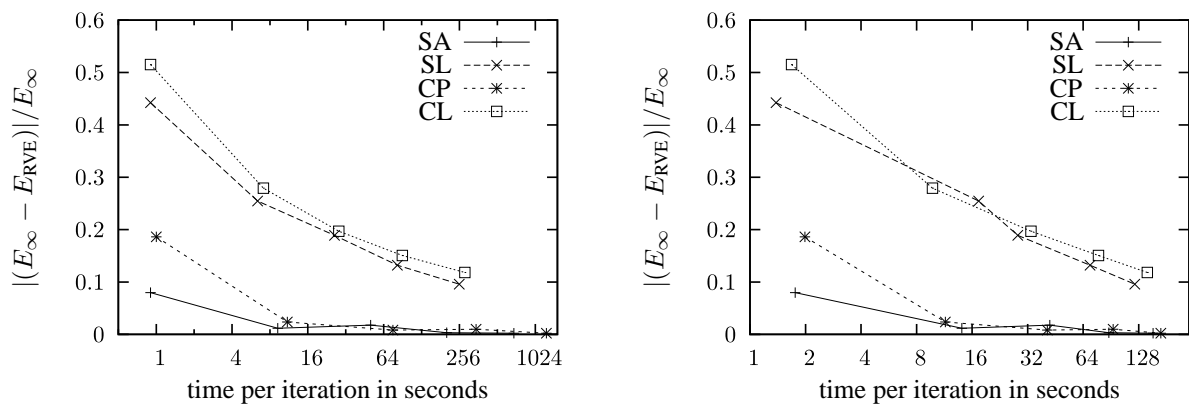


Figure 4: Absolute value of the relative deviation of the RVE Young's modulus from the asymptotic Young's modulus over the numerical expense. In the legend, S and C stand for sphere and cube, while L, P and A stand for linear displacement, periodic and antipodic boundary conditions.

4 Summary

When addressing the question whether the advantage of spherical RVE in terms of surface to volume ratio results in a reduction of computational time, two specific conclusions can be drawn:

In case of periodic/antipodic boundary conditions and the direct solver, the reduced number of surface points leads to a better performance of spherical RVE compared to cubical RVE with a similar number of DOF, since there are less numerically disadvantageous node adjacencies. This advantage is partially cancelled out due to a necessarily irregular meshing of the sphere, when hexahedral elements are used. With a common maximum element size, the spherical RVE require more nodes per volume (namely by a factor of approximately 1.7).

In most situations, one will use the iterative solver and a microstructure-conform meshing, for which none of these two issues plays a role. However, for the multiscale FEM, one is usually restricted to relatively small RVE, where the direct solver is to prefer, and periodic/antipodic boundary conditions, for obtaining reasonable effective properties at small RVE sizes. Then, it seems appropriate to use spherical RVE with antipodic boundary conditions, both due to better convergence in terms of RVE size and a better performance of the direct solver.

References

- Coenen, E. W. C.; Kouznetsova, V. G.; Geers, M. G. D.: Novel boundary conditions for strain localization analyses in microstructural volume elements. *International Journal for Numerical Methods in Engineering*, 90, (2012), 1–21.
- Feyel, F.: Multiscale FE² elastoviscoplastic analysis of composite structures. *Computational Materials Science*, 16, 14, (1999), 344–354.
- Fritzen, F.; Böhlke, T.: Influence of the type of boundary conditions on the numerical properties of unit cell problems. *Technische Mechanik*, 30, 4, (2010a), 354–363.
- Fritzen, F.; Böhlke, T.: Three-dimensional finite element implementation of the nonuniform transformation field analysis. *International Journal for Numerical Methods in Engineering*, 84, (2010b), 803–829.
- Glüge, R.; Weber, M.; Bertram, A.: Comparison of spherical and cubical statistical volume elements with respect to convergence, anisotropy, and localization behavior. *Computational Material Science*, 63, (2012), 91–104.
- Ilic, S.; Hackl, K.: Application of the multiscale FEM to the modeling of nonlinear multiphase materials. *Journal of Theoretical and Applied Mechanics*, 47, 3, (2009), 537–551.
- Kanit, T.; Forest, S.; Galliet, I.; Mounoury, V.; Jeulin, D.: Determination of the size of the representative volume element for random composites: statistical and numerical approach. *International Journal of Solids and Structures*, 40, (2003), 3647–3679.
- Kreikemeier, J.: Modelling of Phase Boundaries via the GAUSS-Point Method. *Technische Mechanik*, 32, 6, (2012), 658–666.

Address: Otto-von-Guericke-Universität Magdeburg, Universitätsplatz 2, D-39104 Magdeburg
email: gluege@ovgu.de, martin.weber@ovgu.de